Chapter

Fracture Behavior of Solid-State Welded Joints

Dattaguru Ananthapadmanaban and
K. Arun Vasantha Geethan

Abstract

The nature of the fractured surface gives information about the type of failure. This chapter focuses on the study of the fractured surfaces. Solid-state welding processes, such as friction welding, friction stir welding, and laser welding, have been used for welding dissimilar joints in recent times. Different combinations of materials and different welding conditions give rise to changes in the morphology of the fractured surfaces. Material combinations that have been chosen in this study are industrially useful combinations such as titanium-stainless steel and aluminum-copper. An attempt has been made to study the fractured interfaces, mainly using scanning electron microscope (SEM). In order to achieve this objective, case studies have been made use of.

Keywords: fracture, solid-state welding, welding parameters, scanning electron micrograph, mode of fracture

1. Introduction

Fracture surfaces have been studied to give information about the nature of failure. There are basically three types of fractured surfaces: ductile fracture, as defined by the cup and cone type of appearance; brittle fracture that has a cleavage type of appearance; and fatigue fracture characterized by beach marks.

Fracture in fusion welding has been studied in detail by many researchers for a few decades, but fracture in solid-state welds has been researched upon only in recent times.

Solid-state welding mainly comprises of friction welding, friction stir welding, and laser and electron-beam welding. This chapter is aimed at studying the fractured surfaces of practical cases of welding dissimilar joints.

2. Methods and materials

The authors start with friction welding since they have worked on this topic for some years now. Friction welding is a solid-state welding technique, which has been in use for the last 20 years. The main input parameters for welding are friction pressure, upset pressure, burn-off length, and speed of rotation. These parameters can be varied to give different qualities of weld joint. It is also seen that the nature of fracture and the place where the fracture occurs differ with varying friction welding parameters.

2.1 Friction welding parameters-stainless steel

Low carbon steel has been friction welded with stainless steel, and fractography for various combinations of friction welding parameters has been reported. Similarly, aluminum has been friction welded with copper, and SEM micrograph has been studied to characterize the type of failure.

The same procedure has been followed for friction stir welding and laser welding. Analysis of friction stir welded joints has been done, both for ferrous welds and nonferrous welds.

Friction welding in the case of low carbon steel-stainless steel has been carried out with the following parameters (**Table 1**).

Table 2 gives the parameters for aluminum-copper friction welds.

Welding of aluminum with copper with nickel interlayer has been carried out with the following parameters as shown below in **Table 3.**

A detailed study by Ahmed et al. [1] showed that while friction stir welding 5052 with 7075 alloys, the optimum parameters used were 1400 rpm tool speed and 200 mm/min transverse speed.

S. No.	Friction pressure (MPa)	Upset pressure (MPa)	Burn-off length (mm)	RPM (rpm)
1	120	180	6	2000
2	120	180	6	1000
3	120	180	2	2000
4	120	180	2	1000
5	120	127.5	6	2000
6	120	127.5	6	1000
7	120	127.5	2	2000
8	120	127.5	2	1000
9	40	180	6	2000
10	40	180	6	1000
11	40	180	2	2000
12	40	180	2	1000
13	40	127.5	6	2000
14	40	127.5	6	1000
15	40	127.5	2	2000
16	40	127.5	2	1000

Table 1.
Friction welding parameters for Low Carbon steel-Stainless Steel combination.

S. No.	Friction pressure (MPa)	Upset pressure (MPa)	Burn-off length (mm)	Speed of rotation (rpm)
1	64	160	2	750
2	80	120	2	1000
3	64	64	2	1000
4	32	96	3	1000

Table 2.
Friction welding parameters for Aluminium-Copper combination.

Friction pressure (MPa)	Upset pressure (MPa)	Upset time (s)	Burn-off length	Spindle speed (rpm)
40	110	3	2	1500
40	130	2.5	2	1500
60	110	2	3	1500
80	95	3.5	3	1600
80	120	3	2	1600

Table 3.
Aluminum to copper with interlayer welding parameters.

3. Results and discussion

3.1 Fractography studies of low carbon steel-stainless steel friction welds

Fractography studies were done on friction welded samples; typical SEM fractographs are shown here. Typical SEM micrograph of a failure in the low carbon steel side is shown [2]. Here, we find the failure to be of a mixed mode (**Figure 1**).

The following SEM images show failure at the weld. The friction welding parameters used are given below.

The following SEM fractographies represent failure in the stainless steel side [2].

Figures 2 and **3** show fairly ductile modes of fracture.

Figures 4 and **5** show brittle mode of fracture. Hence, it can be inferred that the mode of fracture is influenced by the friction welding parameters. More detailed studies may be necessary to come to conclusions on what parameters give ductile failure and which parameters give brittle failure. Mixed mode type of failure is also obtained for certain welding parameters.

A total of 16 experiments have been carried out while friction welding low carbon steel to stainless steel; details of the parameters used are given in the previous section.

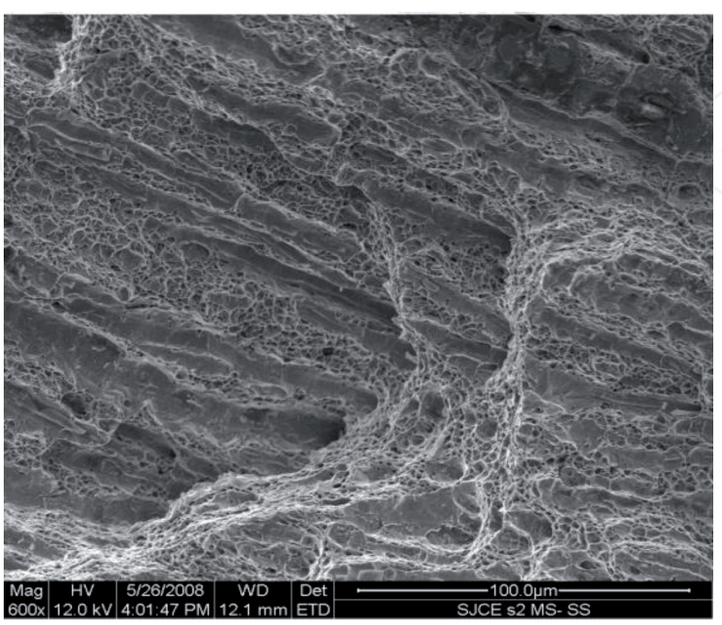

Figure 1.
Friction pressure—120 MPa, upset pressure—180 MPa, burn-off length—6 mm, and speed—2000 rpm.

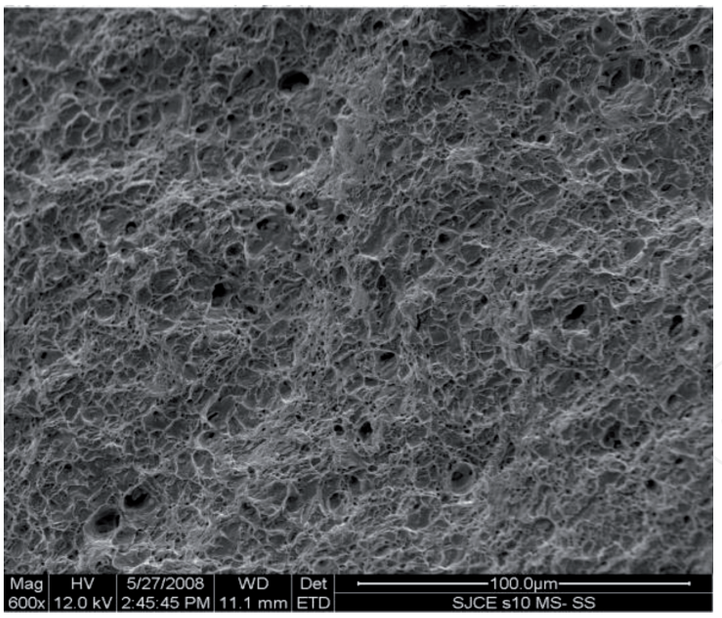

Figure 2.
Friction pressure—40 MPa, upset pressure—180 MPa, burn off length—6 mm, and speed—1000 rpm.

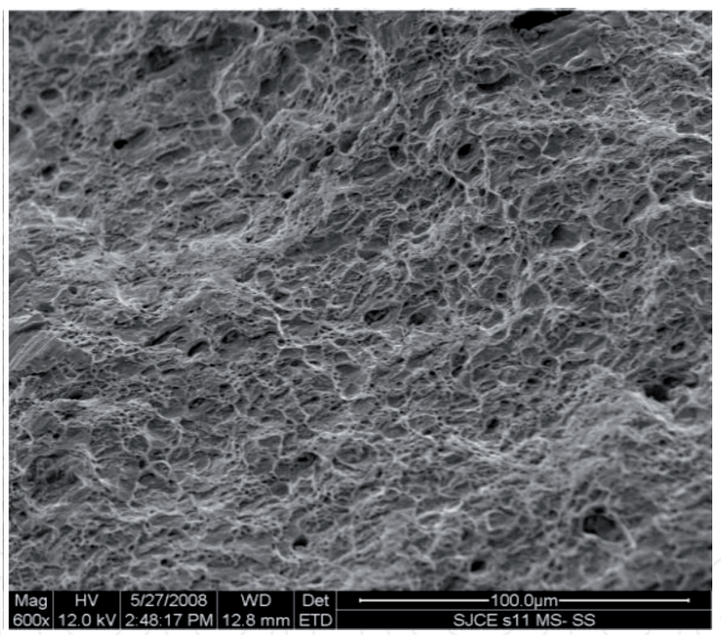

Figure 3.
Friction pressure—40 MPa, upset pressure—180 MPa, burn off length—2 mm, and speed—2000 rpm.

Results of the tensile testing on friction welds are presented in **Table 4**.

Specimens 2–8 failed in the low carbon steel side. Specimens 9–12 failed in the weld. Specimens 13–16 failed on the stainless steel side. Specimens 1–6 also showed a fair deal of ductile behavior. Thus, we can infer that the location of failure depends upon the friction welding parameters used. It will also be of interest to try these sort of experiments for other dissimilar metal combinations.

3.2 Fractography of aluminum-copper friction welds

Aluminum sticks to copper under certain conditions and breaks without any joining under certain different conditions. In all cases, the failure mode observed in the case of aluminum-copper was brittle fracture.

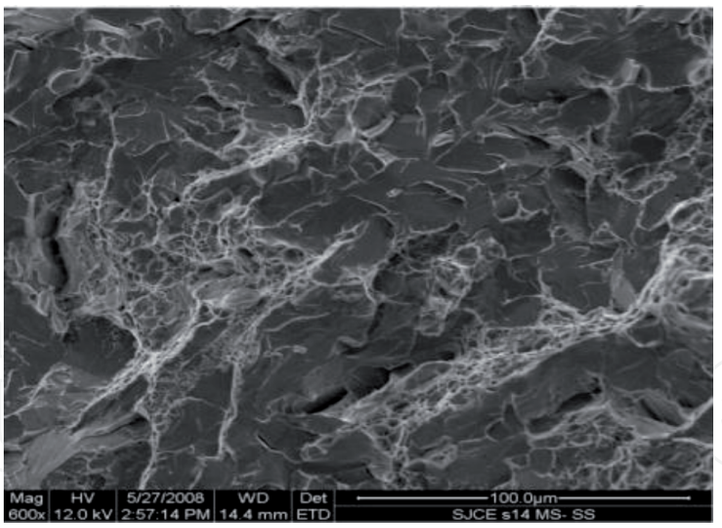

Figure 4.
F.P—40 MPa, U.P—127.5 MPa, BOL—6 mm, and speed–1000 rpm.

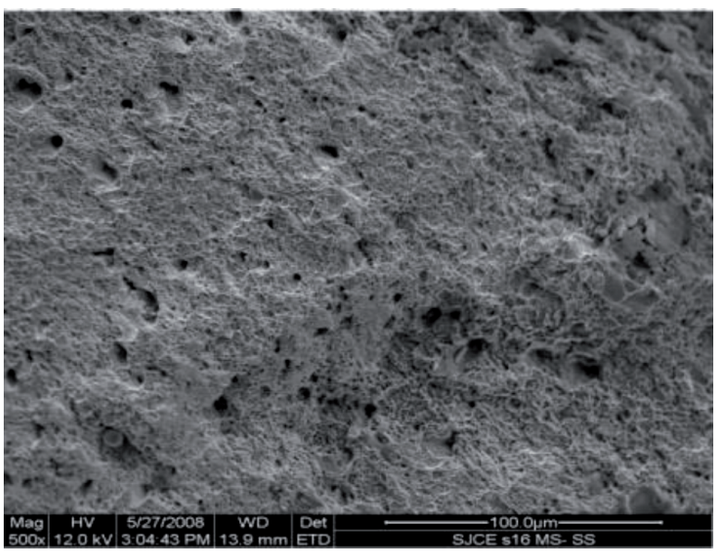

Figure 5.
F.P—40 MPa, U.P—127.5 MPa, BOL—2 mm, and speed—2000 rpm.

SEM studies for aluminum-copper combination were done, and some of the SEM micrographs are shown in **Figures 6–9**.

3.3 Fractography of aluminum-copper with nickel interface

In the photomicrograph of SEM-EDAX for aluminum-copper with nickel interlayer, we can observe that some copper has diffused into the interlayer (**Figure 10**). **Figure 11** shows SEM and EDAX for copper side of the weld. Here, the presence of aluminum is very marginal. It can be concluded that the nickel interlayer was effective in reducing the diffusion of aluminum to the copper side. The two zones showed here are the copper matrix and the nickel interface. The diffusion zone is between the copper and nickel with thin diffusion zone. The nickel matrix is not affected by corrosion process comparing to the copper where some pitting observed. The interface diffusion zone layer is unaffected.

Corrosion studies were also done by Ravikumar et al. on friction welded aluminum to copper with nickel interface, and SEM photographs are presented [3].

S.No.	Tensile strength (MPa)	Fracture location
1	596	Weld
2	609	Low carbon steel side
3	604	Low carbon steel side
4	625	Low carbon steel side
5	585	Low carbon steel side
6	607	Low carbon steel side
7	610	Low carbon steel side
8	632	Low carbon steel side
9	557	Weld
10	578	Weld
11	563	Weld
12	581	Weld
13	542	Weld
14	574	SS side
15	570	Weld
16	464	SS side

Table 4.
Fracture location variation for low carbon steel-AISI304L stainless steel combination.

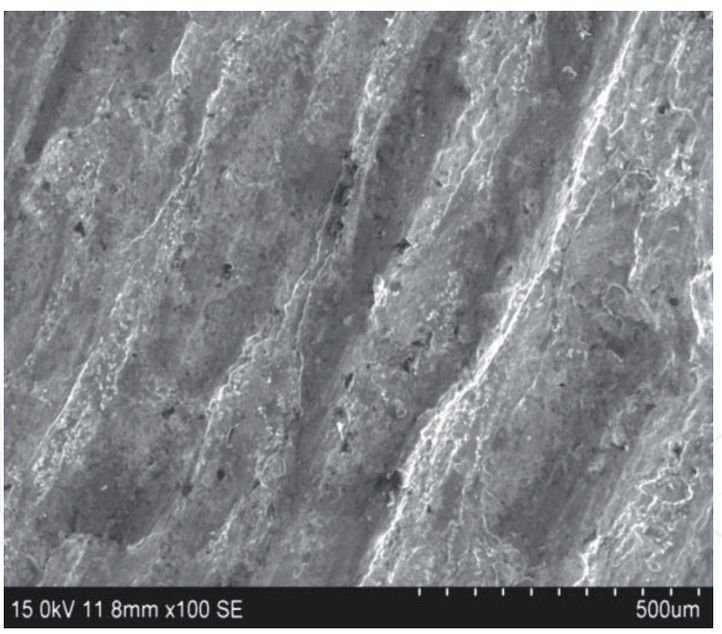

Figure 6.
F.P—64 MPa, U.P—160 MPa, BOL—2 mm, and speed—750 rpm.

Figure 12 shows SEM of the welds with nickel as interlayer after electro-chemical corrosion evaluation tests as per ASTM G 59-97.

3.4 Friction stir welding

Friction stir welding is slightly different from friction welding. It employs a rotating tool to weld two flat weld pieces. The tool chosen depends upon the material combination that is to be welded. Figure shows SEM micrograph of friction stir welded aluminum to steel joints. Ideally, solid-state welding processes, such as friction welding

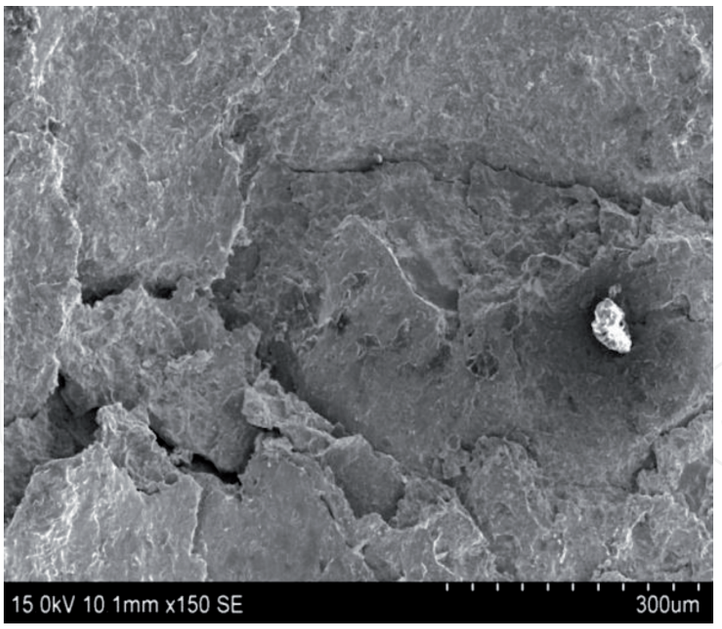

Figure 7.
F.P—80 MPa, U.P—120 MPa, BOL—2 mm, and speed—1000 rpm.

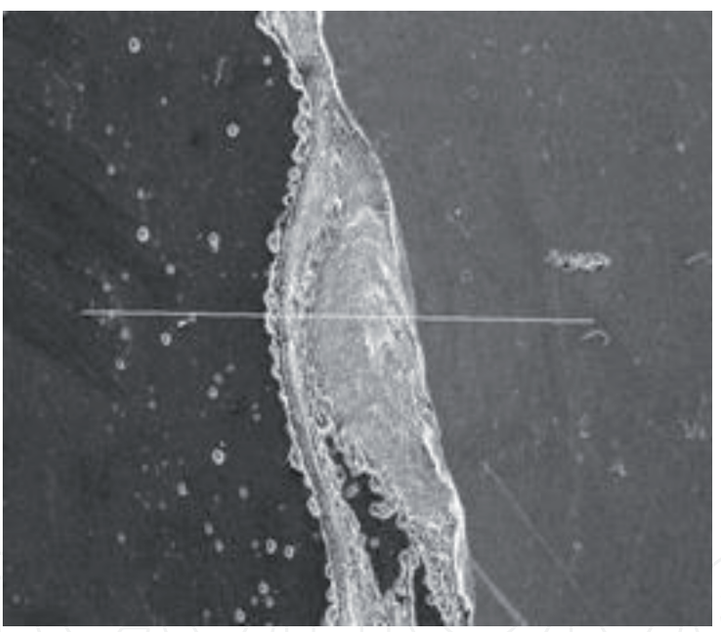

Figure 8.
F.P—64 MPa, U.P—64 MPa, and BOL—2 mm.

and friction stir welding, should not give rise to intermetallics in the weld joints, but in practice, a small amount of intermetallic is seen in the joint as shown below. These intermetallics are detrimental to the properties of the weld and efforts should be made to minimize, if not completely do way with them. This is done by varying the friction stir welding parameters and optimizing them. **Figure 13** shows the SEM photographs of aluminum steel friction stir welded joints. Intermetallic layer can be clearly seen.

3.4.1 Friction stir welding of 5 series and 7 series

These two alloys are commonly used in aircraft applications [5]. In aircraft alloys, fatigue failure is a very common mode of failure. The SEM photographs shown below clearly show striations which are an indication of fatigue failure (**Figure 14**).

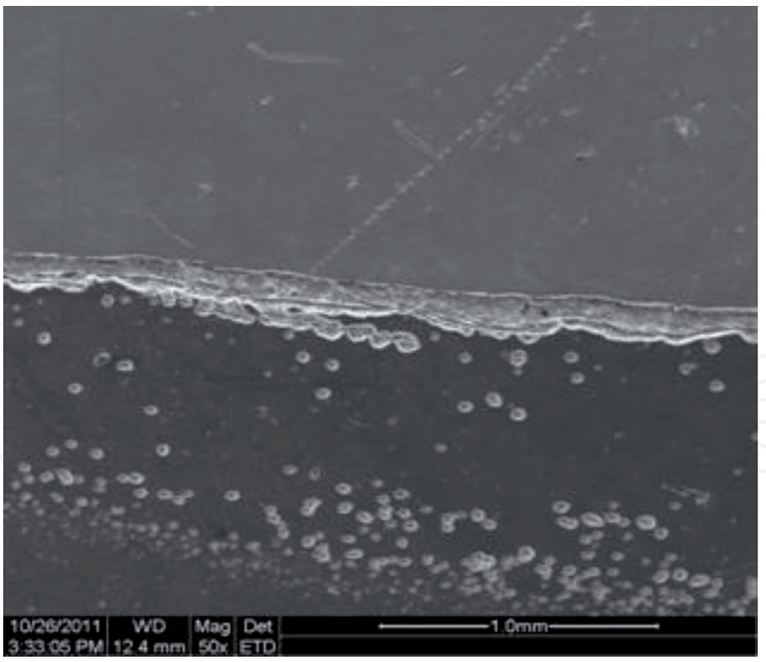

Figure 9.
F.P—32 MPa, U.P—96 MPa, and BOL—3 mm.

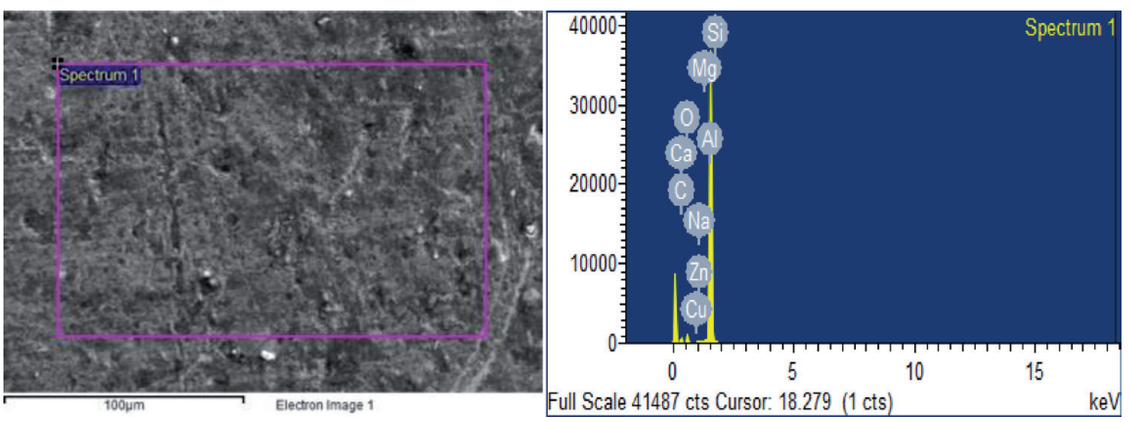

Figure 10.
Fractured surface of Al-Cu with nickel interface.

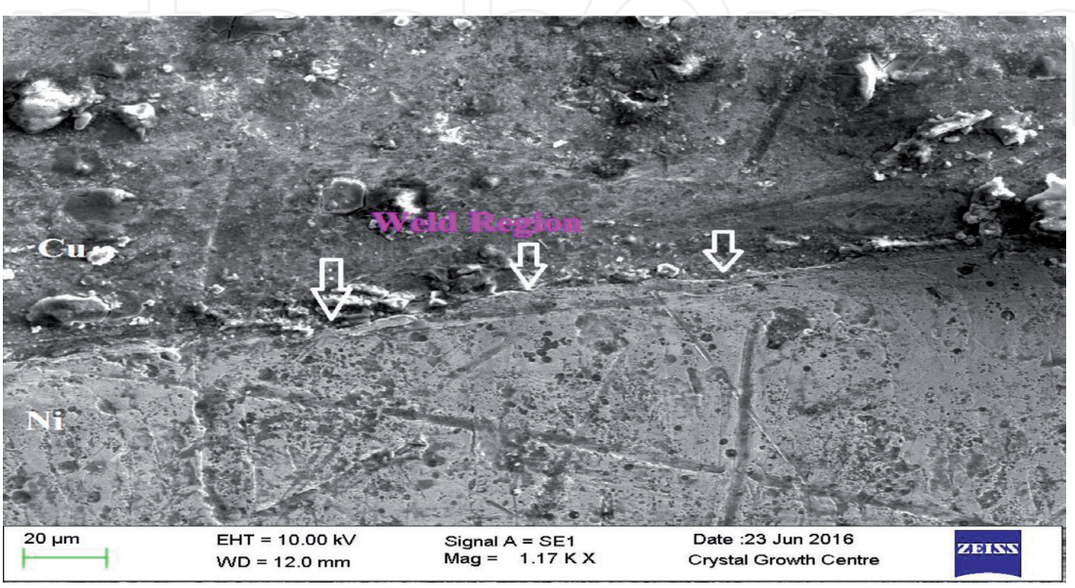

Figure 11.
SEM-EDAX on the copper side of the weld.

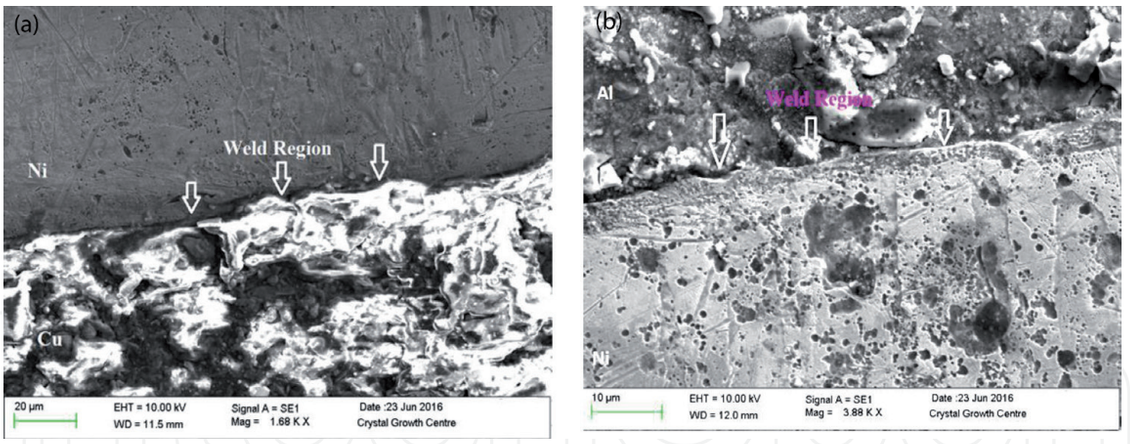

Figure 12.
Interface of specimen welded observed under FESEM at 1000 rpm: (a) copper side and (b) aluminum side.

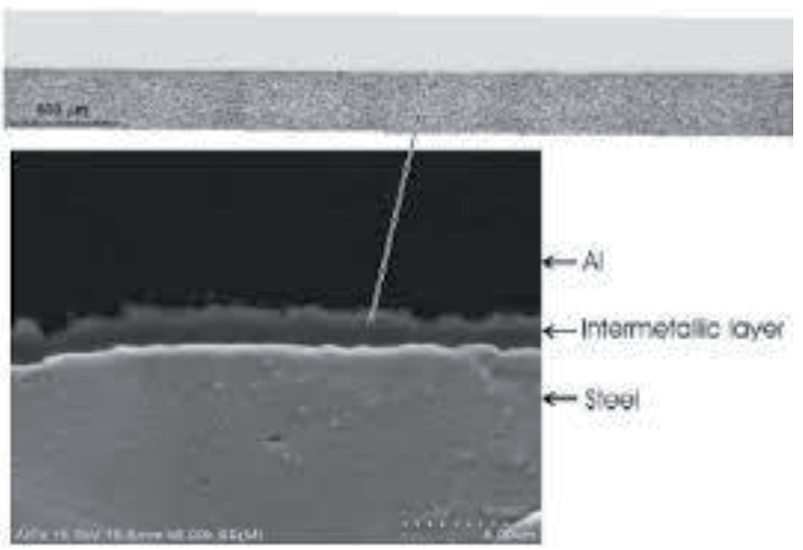

Figure 13.
SEM fractography of friction stir joints, advancing speed 200 mm/min [4].

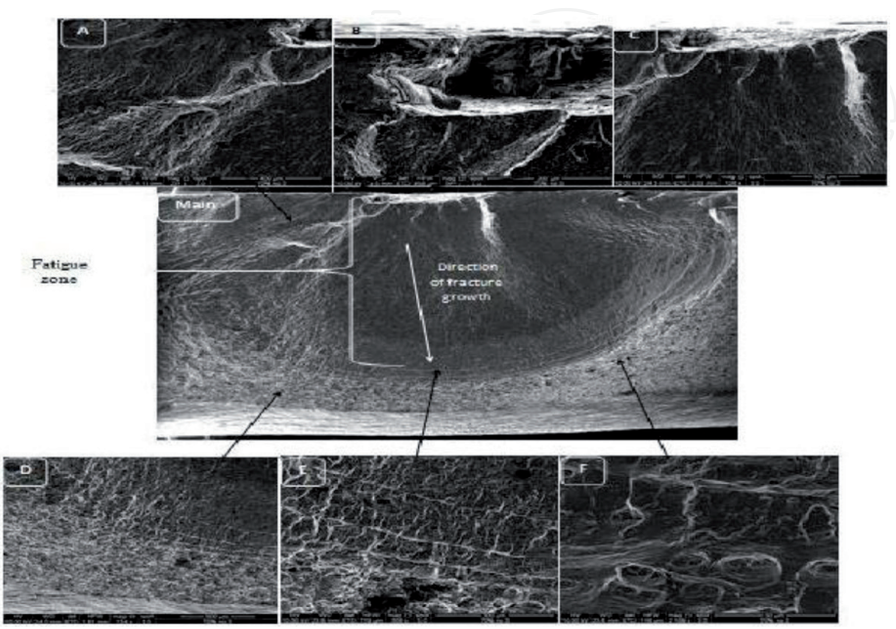

Figure 14.
SEM of 5052 and 7075 alloys—failure by fatigue [1].

It is found that the joint fabricated, using the FSW parameters of 1400 rpm (tool rotational speed) and 20 mm/min (traverse speed), showed higher strength properties compared with other joints, and the SEM shown above represents these set of parameters.

Friction stir welds, such as friction welds, can fail in parent metal or in any of the dissimilar metals. **Figure 15** shown gives the different locations of failure.

Zhang et al. studied the fractured surface of Al 6005 joints. The crack was found in the HAZ zone close to TMAZ. As shown in **Figure 16**, the fracture surface consisted of three regions. The crack initiation zone, which is located at the specimen surface, exhibited a relatively smooth microstructure (**Figure 17**). The crack propagation zone had prominent striation marks with a river-like appearance [7].

The phase of small crack initiation and propagation accounts for about 50–80% of the fatigue life. The growth rate of the major crack is similar to that of other small cracks

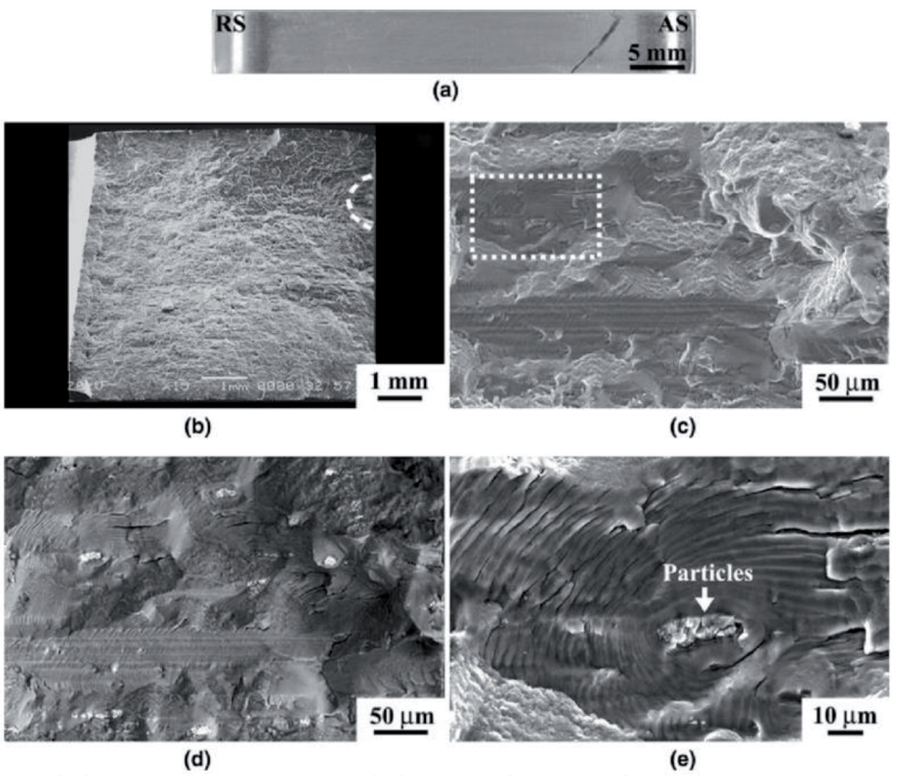

Figure 15.
Different failure locations in friction stir welds [6].

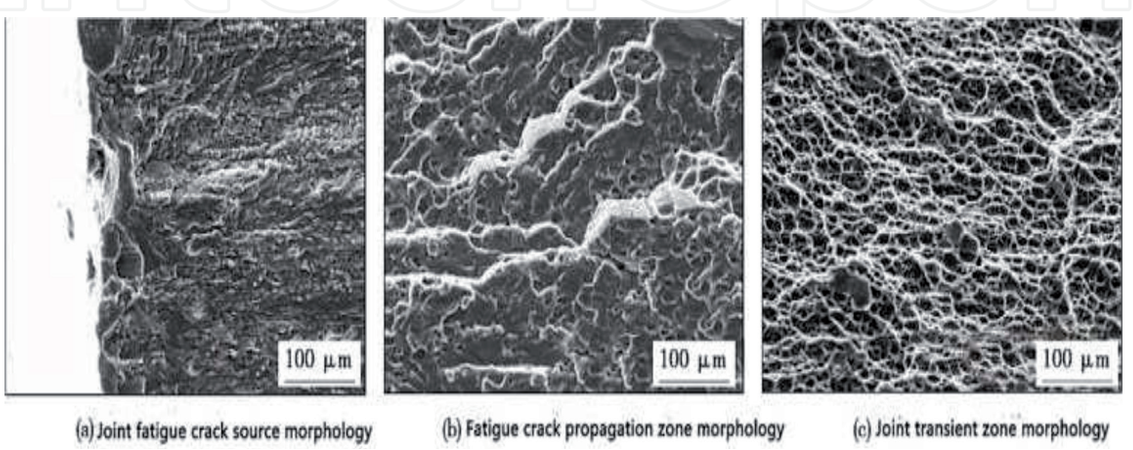

Figure 16.
Fatigue crack propagation in 6005 friction welded joints [7].

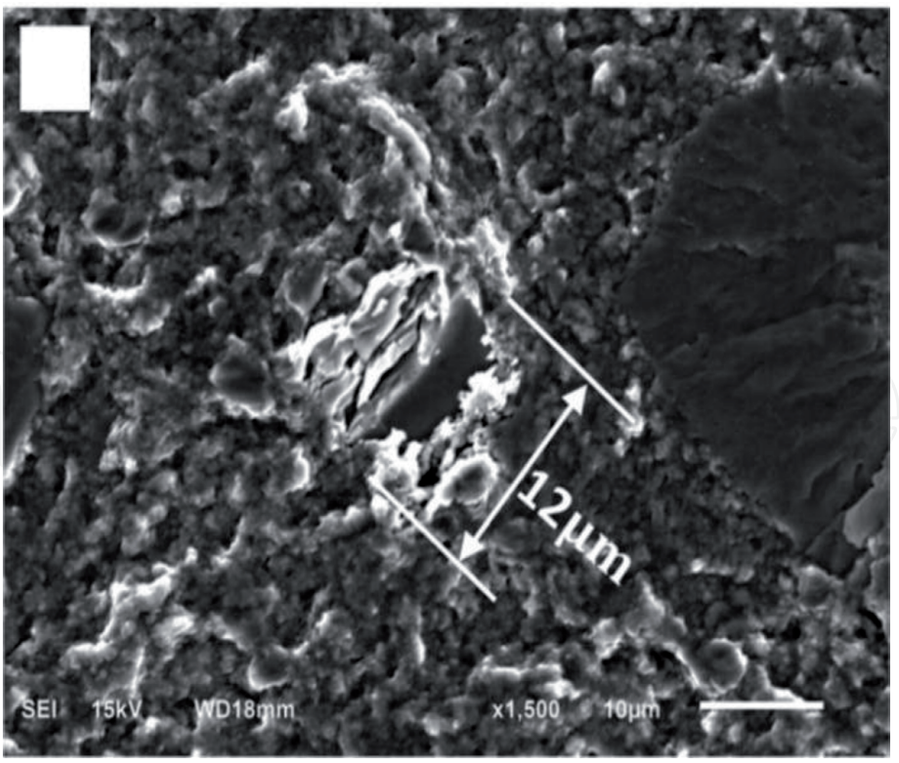

Figure 17.
Details of crack initiation during fatigue failure [8].

in the stage of small cracks growth. In the stage of long cracks growth, the growth rate of the major crack is far greater than that of other small cracks. The microstructures of different regions of the joint have an effect on the fracture mode (**Figure 18**).

3.5 Laser welded joints

Laser welding is also widely being used in recent times, the reason being laser welds have very narrow heat affected zones. This helps in defect-free welds.

3.5.1 Laser welded steels

Unlike friction welds or friction stir welds, SEM micrograph in this case shows a very smooth surface. This can be attributed to the small size of the heat affected zone.

Laser welding has been performed on high grade 960 steel joints [10].

As shown in **Figure 19**, the fracture surface near the specimen surface of BM shows a combination of equiaxed and elongated dimples, indicating that the shearing motion occurs. However, welded joints show quasi-cleavage fracture. Fracture is layered features (as shown in **Figure 19**). The tensile fracture surfaces of BM and welded joint show mostly equiaxed dimples at the center indicating ductile fracture characteristics. Cup-like dimple rupture is the main feature of the fracture surface, representing ductile type of fracture mode (**Figure 20**).

3.5.2 Laser welded nonferrous alloy

The case study taken here is the welding of aluminum alloy 6022 with zinc alloy AZ 31. Fusion zone can be clearly seen. The two base metals can also be seen. An nickel interlayer has been added in this case, which as we have seen earlier results in better corrosion resistance.

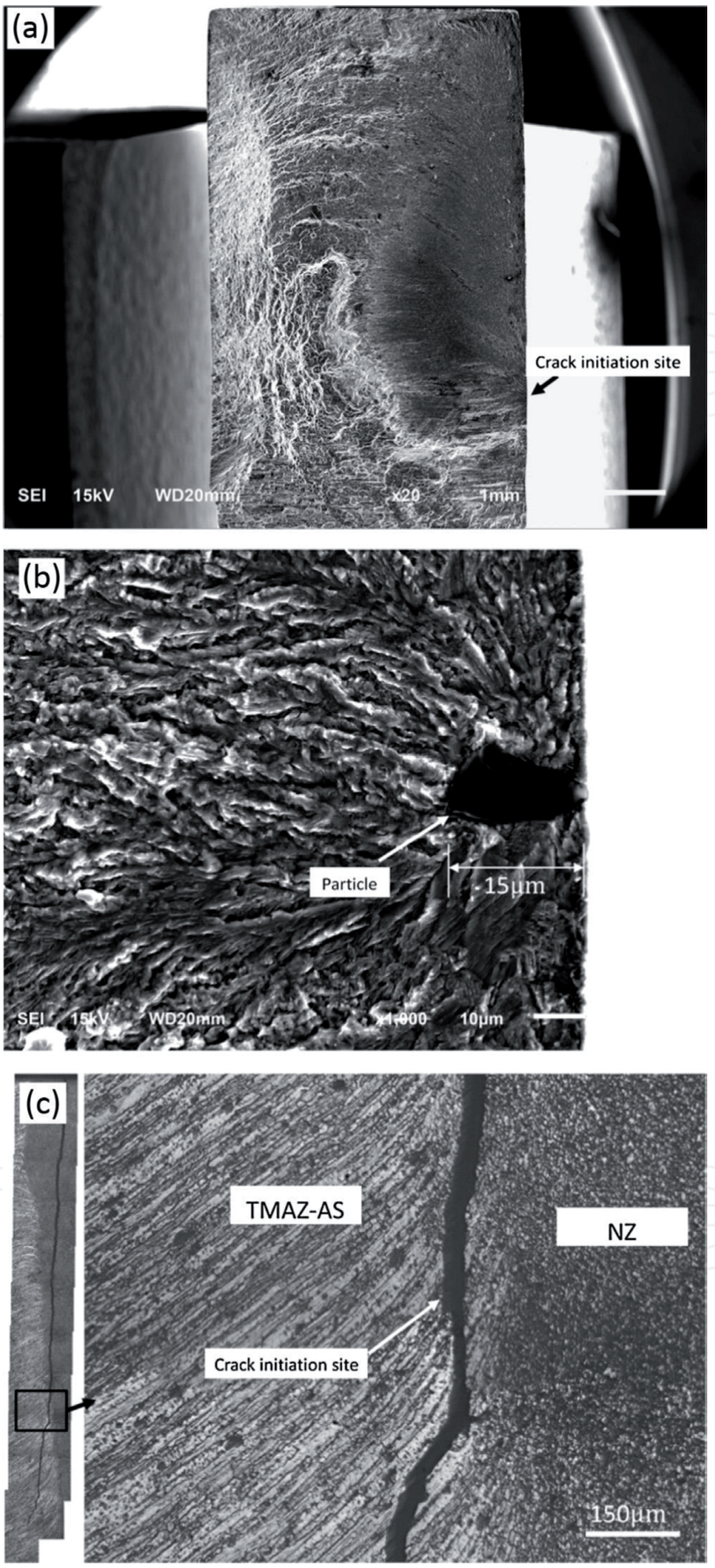

Figure 18.
SEM and OM observation of typical crack initiation site at the TMAZ-AS (Nf = 1.45 06 cycles, rb = 90 MPa). (a) The crack initiating at the specimen surface. (b) Enlargement of the fatigue crack initiation site showing a dark particle. (c) The crack locating at the TMAZ closed to the NZ [9].

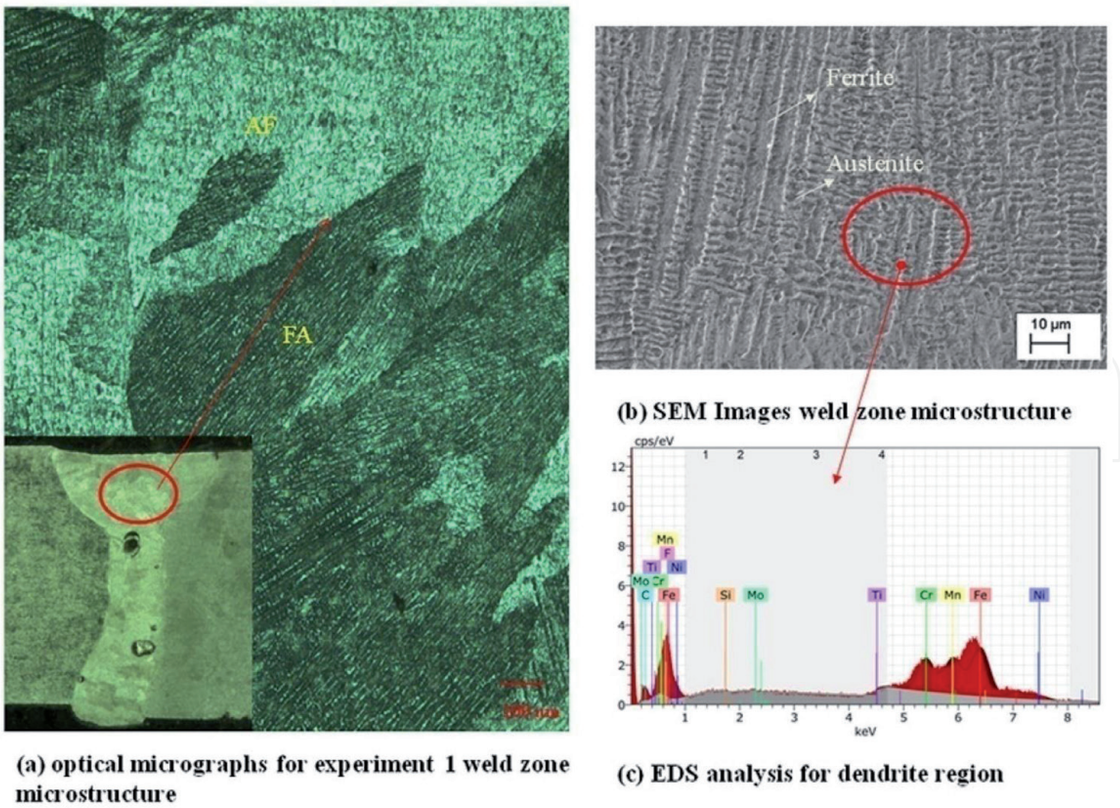

(a) optical micrographs for experiment 1 weld zone microstructure

(b) SEM Images weld zone microstructure

(c) EDS analysis for dendrite region

Figure 19.
SEM micrograph of laser welds of steel.

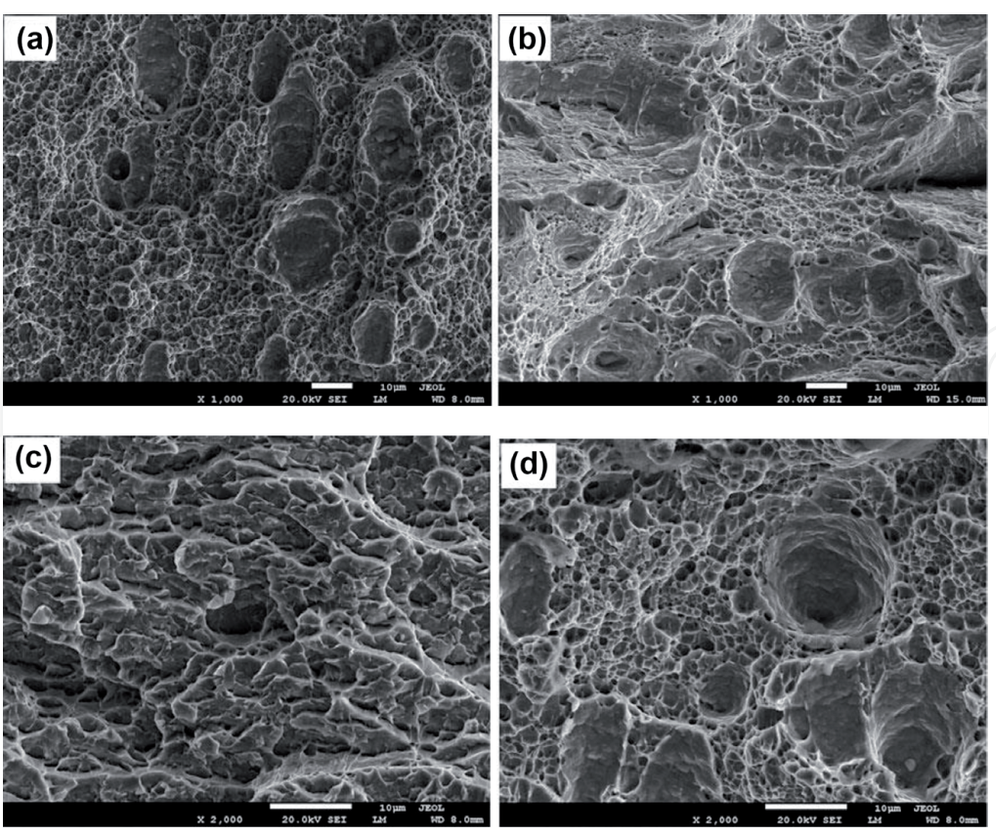

Figure 20.
(a–d) SEM images of tensile facture surface of base metal and welded joints, respectively.

Another case study is the welding of superelastic materials by laser welding. Superelastic NiTi alloy and CuAlMn shape memory alloy have been welded using laser

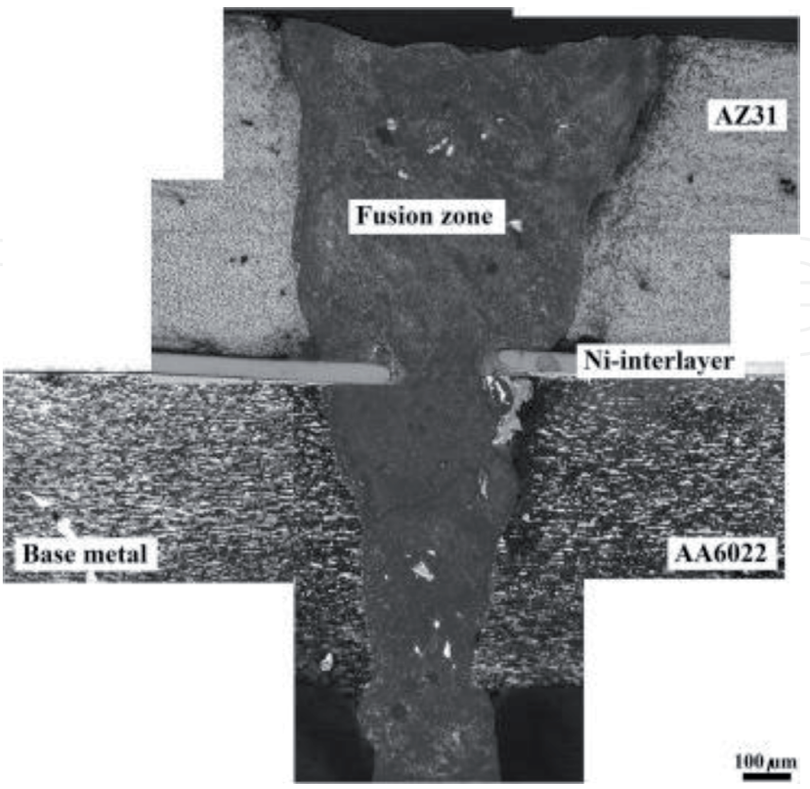

Figure 21.
Laser welds of aluminum-based alloys.

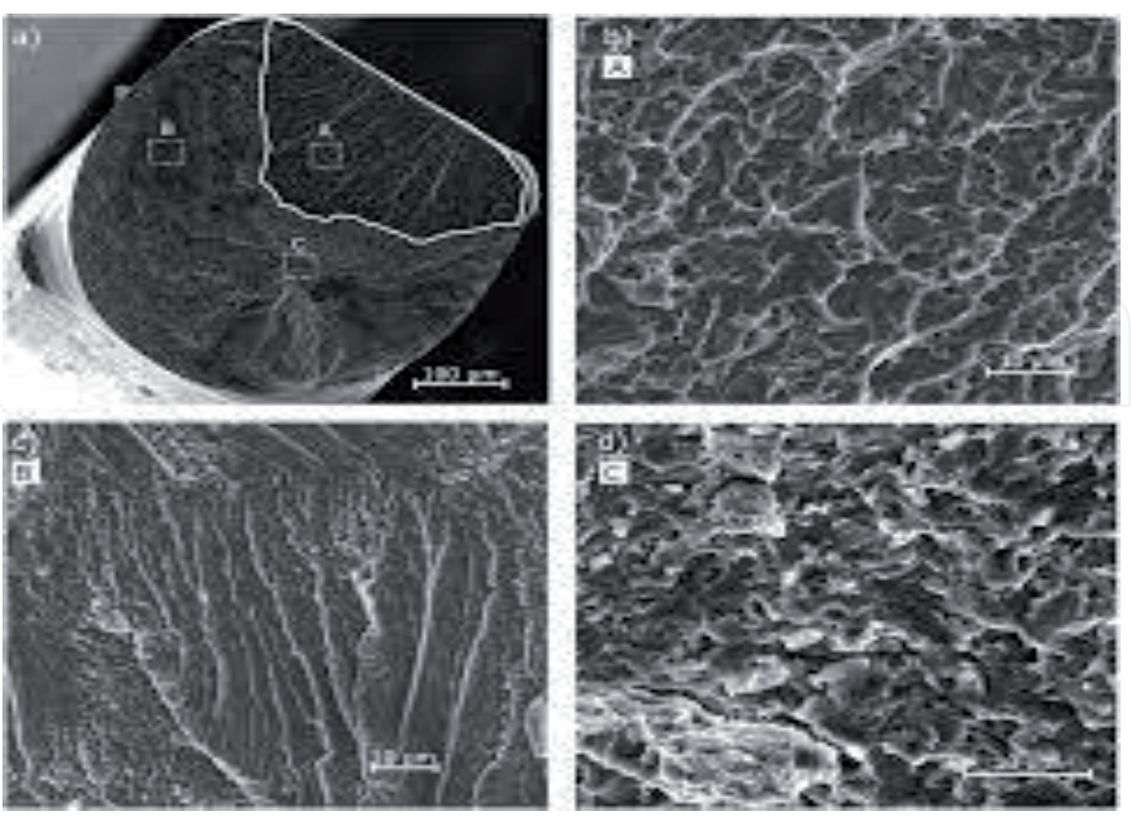

Figure 22.
Laser welded NiTi and CuAlMn [11].

welding. Laser welding has been performed using an Nd-YAG system. The nature of the fractured surface could vary depending upon the system used and the laser welding parameters. For example, when fiber lasers are used, fracture surface may change.

In this case, as shown in **Figure 21**, ductile failure can be seen as also a clear cup and cone type of appearance, which is the characteristic of ductile failure.

Fatigue crack growth behavior can be studied, and SEM micrographs taken in order to get more information about crack growth in dissimilar materials. A comprehensive

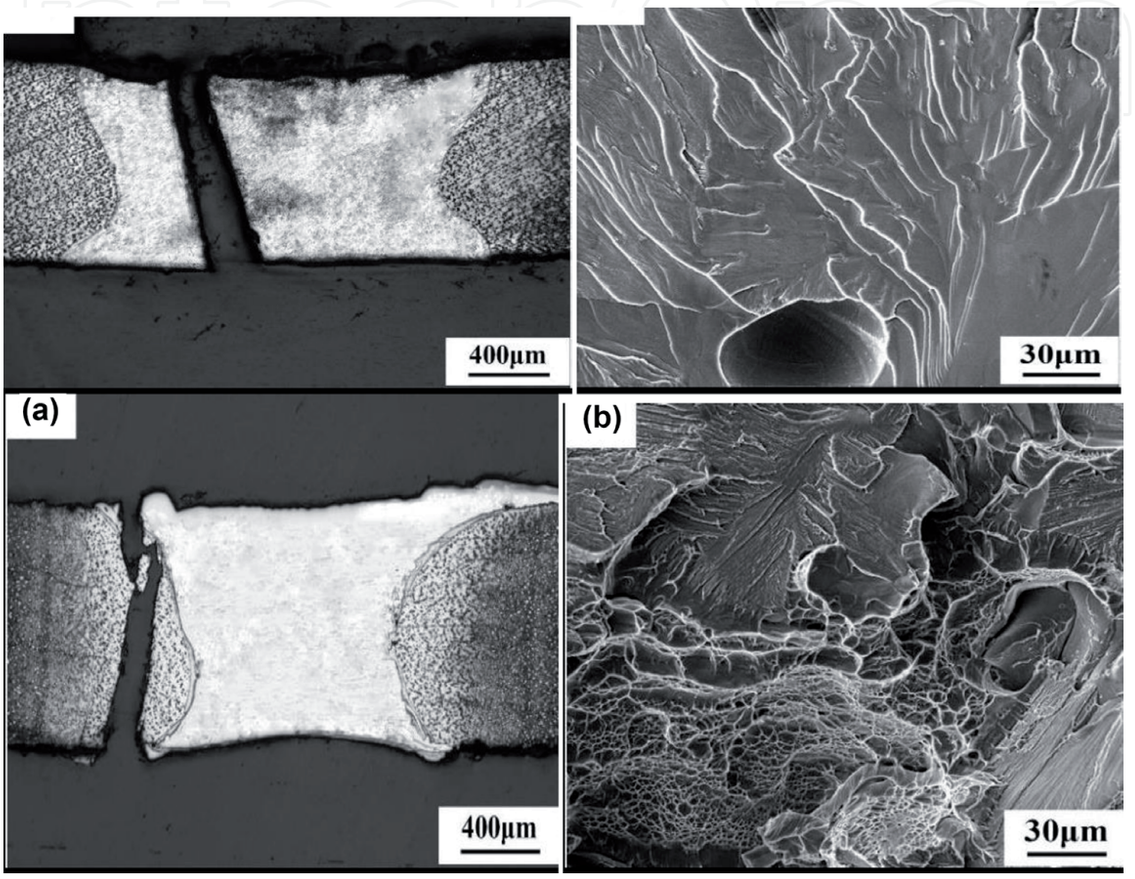

Figure 23.
(a) The fracture path and (b) fracture surface morphology of the joint without filler metal.

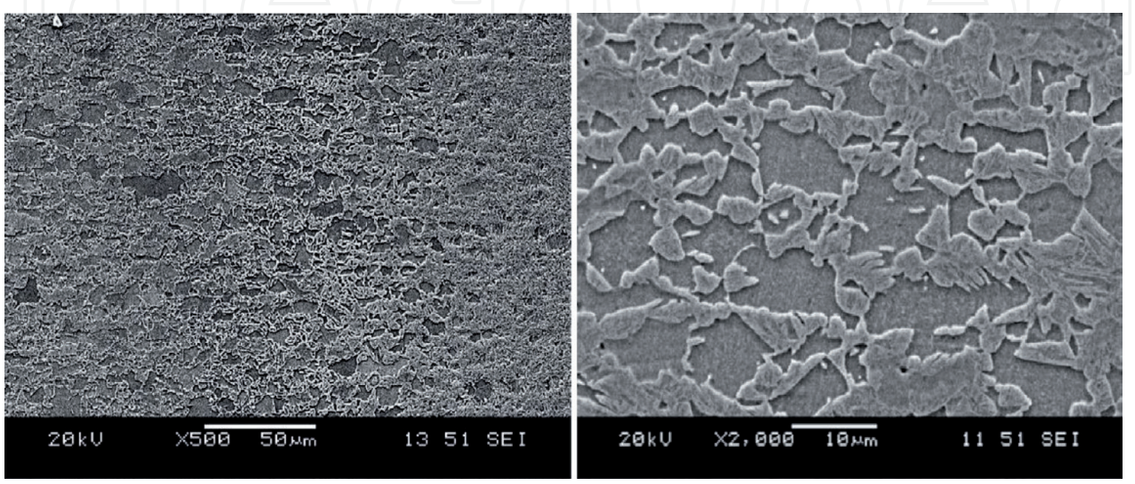

Figure 24.
SEM of fiber laser welds—1 kW fiber laser with 1000 W average output power.

study has been done by Malarvizhi and Balasubramaniam [12]. A good overview of different laser welding processes has been given by Pengfei Wang [13] (**Figure 22**).

Figure 23 show Ti3 Al-Nb laser welds with and without Nb filler. It is seen that Nb filler contributes a lot to ductile behavior as seen below.

Figure 23 shows the fracture path and fracture surface morphology of the joint with Nb filler metal, which is different from those shown in **Figure 12**. The crack was initiated at the weld toe due to generating stress concentration under tensile stress and propagated in HAZ1. The fracture surface also had some cleavage fracture features, but fine dimples and tear-shaped marks along the dimple boundaries were observed (**Figure 13b**). Therefore, the significant enhancement of the joint properties is mainly attributed to the Nb filler metal improving the weld microstructure.

3.5.3 Fiber laser welds

Fiber laser welds show two distinct zones—the intercritical and subcritical HAZ [14–16] (**Figure 24**).

4. Conclusions

This chapter has discussed the scenarios prevailing during fracture of friction welded, friction stir welded, and laser welded joints. A few case studies have been researched upon, both from the author's earlier work and the work of other researchers in the field of solid-state welding. The SEM micrographs' morphologies have been studied, and different fracture surfaces under various conditions of welding have been identified. It is found that the mode of fracture strongly depends upon the welding conditions.

Author details

Dattaguru Ananthapadmanaban[1*] and K. Arun Vasantha Geethan[2]

1 Department of Mechanical Engineering, SSN College of Engineering, Kalavakkam, India

2 Department of Mechanical Engineering, St. Josephs Institute of Technology, Chennai, India

*Address all correspondence to: ananthapadmanaban.dattaguru@gmail.com

References

[1] Zainulabdeen AA, Abbass MK. Investigation of fatigue behaviour and fractography of dissimilar friction stir welded joints of aluminum alloys 7075-T6 and 5052-H34. International Journal of Materials Science and Engineering. December 2014;**2**(2):115-121

[2] Ananthapadmanaban D. PhD thesis. Sathyabama University; 2013

[3] Ravikumar E. PhD thesis. Sathyabama University; July 2019

[4] Shubhavardhana RN, Surendran S. Microstructure and fracture behavior of friction stir lap welding of dissimilar metals. Engineering Solid Mechanics. 2018:**72019**

[5] Vijayakumar R, Kannan V, Natarajan A. Friction Stir Welding of Aluminium Alloys. IntechOpen; 2017. pp. 81-98

[6] Feng AH, Chen D, Ma ZY. Microstructure and cyclic deformation behaviour of a friction-stir-welded 7075 Al alloy. Metallurgical and Materials Transactions A. April 2010;**41a**:957

[7] Zhang K, Fang Y, Luan G, Zhang J, Hu F. Mechanical and fatigue property of stationary shoulder friction stir welding AA6005. Transactions of the China Welding Institution. 2017;**38**:25-28

[8] He C, Liu Y, Dong J, Wang Q, Wagner D, Bathias C. Fatigue crack initiation behaviors throughout friction stir welded joints in AA7075-T6 in ultrasonic fatigue. International Journal of Fatigue. 2015;**81**:171-178

[9] He C, Liu Y, Dong J, Wang Q, Wagner D, Bathias C. Fatigue crack initiation behaviors throughout friction stir welded joints in AA7075-T6 in ultrasonic fatigue. HAL Archives. January 2018

[10] Oliveira JP, Zeng Z, Andrei C, Braz Fernandes FM, Miranda RM, Ramirez AJ, et al. Dissimilar laser welding of superelastic NiTi and CuAlMn shape memory alloys. Materials & Design. 2017;**128**:166-175

[11] Meng W, Li Z, Huang J, Wu Y, Katayama S. Microstructure and softening of laser-welded 960 MPa grade high strength steel joints. Journal of Materials Engineering and Performance. 2014;**23**:538-544

[12] Malarvizhi S, Balasubramanian V. Fatigue crack growth resistance of gas tungsten arc, electron beam and friction stir welded joints of AA2219 aluminium alloy. Materials and Design. 2011;**32**:1205-1214

[13] Wang P, Chen X, Pan Q, Madigan B, Long J. Laser welding dissimilar materials of aluminum to steel: An overview. The International Journal of Advanced Manufacturing Technology. December 2016;**87**(9-12):3081-3090

[14] Parkes D, Xua W, Westerbaan D, Nayak SS, Zhou Y, Goodwin F, et al. Microstructure and fatigue properties of fiber laser welded dissimilar joints between high strength low alloy and dual-phase steels. Materials and Design. 2013;**51**:665-675

[15] Ravikumar E, Arunkumar N, Anathapadmanaban A, Prabhakaran V. Corrosion Studies on Friction Welded Aluminium Alloy AA6061-T6 to Copper with Nickel Interlayer, Advances in Manufacturing Processes. Lecture Series in Mechanical Engineering. Springer; September 2018

[16] Khodabakhshi F, Shah LH, Gerlich AP. Dissimilar laser welding of an AA6022-AZ31 lap-joint by using Ni-interlayer: Novel beam-wobbling technique, processing parameters, and metallurgical characterization. Optics & Laser Technology. April 2019;**112**(15):349-362